Author Manuscript

Author Manuscript

Author Manuscript

Author Manuscript

HHS Public Access

Author manuscript

*Cancer Res*. Author manuscript; available in PMC 2023 March 02.

Published in final edited form as:

*Cancer Res*. 2022 September 02; 82(17): 3158–3171. doi:10.1158/0008-5472.CAN-22-0170.

# Retinoic acid receptor activation reduces metastatic prostate cancer bone lesions by blocking the endothelial-to-osteoblast transition

**Guoyu Yu**[1,+], **Paul G. Corn**[2,+], **Pengfei Shen**[1], **Jian H. Song**[2], **Yu-Chen Lee**[1], **Song-Chang Lin**[1], **Jing Pan**[2], **Sandeep K. Agarwal**[4], **Theocharis Panaretakis**[2], **Maurizio Pacifici**[3], **Christopher J. Logothetis**[2], **Li-Yuan Yu-Lee**[4,*], **Sue-Hwa Lin**[1,2,5,*]

[1]Department of Translational Molecular Pathology, The University of Texas M. D. Anderson Cancer Center; Houston, Texas 77030

[2]Department of Genitourinary Medical Oncology, The University of Texas M. D. Anderson Cancer Center; Houston, Texas 77030

[3]Translational Research Program in Pediatric Orthopaedics, The Children's Hospital of Philadelphia; Philadelphia

[4]Department of Medicine, Section of Immunology Allergy & Rheumatology, Baylor College of Medicine; Houston, Texas 77030

[5]The University of Texas Graduate School of Biomedical Sciences at Houston; Houston, Texas.

## Abstract

Metastatic prostate cancer (PCa) in the bone induces bone-forming lesions that contribute to progression and therapy resistance. PCa-induced bone originates from endothelial cells (EC) that have undergone endothelial-to-osteoblast (EC-to-OSB) transition in response to tumor-secreted BMP4. Current strategies targeting PCa-induced bone formation are lacking. Here, we show that activation of retinoic acid receptor (RAR) inhibits EC-to-OSB transition and reduces PCa-induced bone formation. Treatment with palovarotene, an RARγ agonist being tested for heterotopic ossification in fibrodysplasia ossificans progressiva, inhibited EC-to-OSB transition and osteoblast mineralization in vitro and decreased tumor-induced bone formation and tumor growth in several osteogenic PCa models, and similar effects were observed with the pan-RAR agonist ATRA. Knockdown of RARα, β, or γ isoforms in ECs blocked BMP4-induced EC-to-OSB transition and

*Co-Corresponding authors: Dr. Sue-Hwa Lin, Department of Translational Molecular Pathology, The University of Texas M. D. Anderson Cancer Center, 1515 Holcombe Blvd., Houston, TX 77030. Phone: 713-794-1559; Fax: 713-834-6084; slin@mdanderson.org; Dr. Li-yuan Yu-Lee, Department of Medicine, Section of Immunology Allergy & Rheumatology, Baylor College of Medicine, One Baylor Plaza, Houston, TX 77030. Phone: 713-798-4770; yulee@bcm.edu.

+These authors contributed equally to this work

Author contributions

G.Y., P.G.C., C.J.L., L.-Y.Y.-L., S.-H.L. conceived the idea, planned the experiments, and wrote the manuscript. G.Y., P.S., J.H.S., Y.-C.L., S.-C.L., J.P. carried out the experiments. G.Y, P.G.C., S.K.A, T.P., M.P., L.-Y.Y.-L., S.-H.L. performed data analysis and interpretation. G.Y., C.J.L., L.-Y.Y.-L., S.-H.L. provided scientific inputs for the development of the project. All the co-authors critically reviewed the present manuscript before submission.

Conflict of interest

C. J. Logothetis reports receiving commercial research grants from Janssen, ORIC Pharmaceuticals, Novartis, Aragon Pharmaceuticals; and honoraria from Merck, Sharp & Dohme, Bayer, Amgen. No potential conflicts of interest are disclosed by the other authors.

Author Manuscript Author Manuscript Author Manuscript Author Manuscript

osteoblast mineralization, indicating a role for all three isoforms in PCa-induced bone formation. Furthermore, treatment with palovarotene or ATRA reduced plasma Tenascin C, a factor secreted from EC-OSB cells, which may be used to monitor treatment response. Mechanistically, BMP4-activated pSmad1 formed a complex with RAR in the nucleus of ECs to activate EC-to-OSB transition. RAR activation by palovarotene or ATRA caused pSmad1 degradation by recruiting the E3-ubiquitin ligase Smurf1 to the nuclear pSmad1/RARγ complex, thus blocking EC-to-OSB transition. Collectively, these findings suggest that palovarotene can be repurposed to target PCa-induced bone formation to improve clinical outcomes for patients with bone metastasis.

### Keywords

Bone metastasis; prostate cancer; tumor-induced bone; EC-to-OSB transition; retinoic acid receptor agonists

## Introduction

Metastatic progression in bone signifies the lethal progression of advanced prostate cancer (PCa). Currently approved therapeutic agents for PCa bone metastasis only modestly affect patient survival (1). Thus, there is an urgent need to develop strategies that improve therapy outcomes. PCa bone metastasis is frequently associated with osteoblastic bone-forming lesions (2), indicative of cross-talk between metastatic tumor cells and the stromal component within the tumor microenvironment. We and others have shown that BMPs secreted from PCa cells are involved in the formation of bone lesions in PCa bone metastasis. First, in human-derived osteoblastic PDX MDA PCa-118b, we identified BMP4 by cytokine array as a factor that promotes ectopic bone formation of MDA PCa-118b (3). Second, in human PCa specimens, we found that BMP4 expression was low in 15 of 15 primary PCa specimens, but significantly higher in tumor cells in 10 of 12 needle biopsies of bone metastasis (4). Third, Nordstand et al. (5) showed that BMP4 is expressed in human PCa bone metastasis specimens and BMP4 expression correlates with increased bone formation. Fourth, Dai et al (6) showed that BMP6 contributes to the bone-forming phenotype of PCa bone metastasis. Moreover, Morrissey et al. showed that BMP7 (7) is highly expressed in bone metastasis. At present, the mechanism that leads to the upregulation of BMPs in PCa bone metastasis is not clear. Dai et al.(8) reported that Wnt3a and Wnt5a induce BMP4 and BMP6 expression in PCa cells. Morrissey et al. (7) showed that BMP7 levels are increased in castrate-resistant PCa. Nordstrand et al. (5) showed that high BMP signaling inversely correlates with low tumor cell AR activity in human PCa bone metastasis. Whether androgen depletion therapy leads to BMP upregulation in PCa cells requires further investigation.

A role of osteoblasts (OSBs) in PCa progression in bone was demonstrated by Lin et al. (4), which showed that reduction of tumor-induced bone formation decreased osteogenic tumor growth in a genetically-modified mouse model (4). In addition, inhibition of tumor-induced bone formation, by the BMP receptor inhibitor LDN-193189 (3) or an anti-BMP6 antibody (9), also reduced tumor growth in mouse models. Consistent with this notion, bone-targeting radionuclides, including Sr89 and Samarium-153 EDTMP, were developed

Author Manuscript Author Manuscript Author Manuscript Author Manuscript

for PCa bone metastasis, but significant bone marrow suppression limited their clinical use (10). Radium-223, a bone targeting alpha emitter that remodels bone by inducing cell death in bone microenvironment, increases survival, albeit modest, of patients with bone metastasis (11). As PCa-induced bone formation also increases therapy resistance (12), inhibition of tumor-induced bone formation may improve therapy outcome.

The mechanism of PCa-induced aberrant bone formation was thought to result from the expansion of existing OSBs. However, we recently elucidated an alternative mechanism whereby PCa-induced aberrant bone formation occurs via endothelial-to-osteoblast (EC-to-OSB) transition mediated by tumor-secreted BMP4 (4). We showed that the tumor-associated OSBs in PCa bone metastasis specimens and patient-derived xenografts (PDX) co-express endothelial marker Tie-2 and OSB marker osteocalcin (4); BMP4 promoted EC-to-OSB transition of 2H11 ECs (4); BMP4-overexpression in non-osteogenic C4-2b PCa cells led to ectopic bone formation under subcutaneous implantation (4); and tumor-induced bone was reduced in trigenic mice ($Tie2^{cre}/Osx^{f/f}/SCID$) with EC-specific deletion of OSB cell-fate determinant OSX when compared to that in bigenic mice ($Osx^{f/f}/SCID$) (4). Targeting this unique EC-to-OSB transition may reduce PCa-induced bone formation.

This new understanding of EC-to-OSB transition in PCa–induced bone formation has revealed similarities in the mechanism(s) of PCa–induced bone and ectopic bone arising from the genetic disease fibrodysplasia ossificans progressiva (FOP), also known as stoneman disease (13,14). FOP is a rare genetic disorder in which muscle and connective tissues are gradually replaced by bone, forming bone outside the skeleton (heterotopic ossification). FOP is caused by a hereditary gain-of-function genetic mutation (R206H) in the BMP type I receptor ALK2 (15,16). Mechanistically, the cell source for ectopic bone formation is shown to be ECs that undergo endothelial-to-mesenchymal transition (EndoMT) to become mesenchymal stem cells, which further differentiate into bone tissues (13). Thus, in both diseases the aberrant bone originates from ECs with over-activated BMP signaling. We posit that therapies to prevent heterotopic ossification in FOP could be repurposed for inhibiting PCa–induced aberrant bone formation.

Various strategies have been developed for the treatment of FOP, with most targeting the ALK2 mutation (R206H) (17). Recently, Shimono et al. (18) showed that compounds that activate the nuclear receptor, retinoic acid receptor gamma (RARγ), are effective in inhibiting chondrogenesis and preventing heterotopic ossification in FOP. As cartilage development normally requires an un-liganded RARγ repressor function, the presence of ligands (RARγ agonists) may interfere with transcriptional programming for chondrogenesis and osteogenesis (19). Currently, palovarotene (Palo) is being evaluated as therapy for FOP patients in a phase III clinical trial (NCT03312634). Palo may be repurposed to inhibit PCa–induced aberrant bone formation.

RARγ acts as a transcriptional repressor by recruiting co-repressors to target promoters in the absence of ligands. When ligands are present, RARγ interacts with coactivators to activate gene transcription (20,21). Retinoic signaling plays a critical role in modulating skeletal development (22-24). Overexpression of RARα in transgenic animals leads to appendicular skeletal defects (25). A loss of retinoid receptor–mediated signaling is

Author Manuscript Author Manuscript Author Manuscript Author Manuscript

necessary and sufficient for expression of bone phenotype (26). Thus, retinoic acid signaling inhibits skeletal progenitor differentiation (24).

In this study, we examined whether Palo may be repurposed to inhibit PCa–induced aberrant bone formation. We used MDA-PCa-118b, which is a human-derived PDX endogenously expresses BMP4, as well as PCa cells engineered to overexpress BMP4 in our study. We found that RAR agonists, including Palo and all-trans-retinoic acid (ATRA) inhibit BMP4-induced EC-to-OSB transition and bone formation. In addition, RARs regulate BMP4-induced EC-to-OSB transition through a non-canonical RAR mechanism that is independent of RAR's transcription function. Further, we found that plasma levels of Tenascin C, a protein secreted by EC-OSB cells, can be used for monitoring treatment response. ATRA treatment also does not lead to unwanted bone loss in healthy non-tumor-bearing bones. Thus, Palo and ATRA represent new agents for the treatment of osteoblastic bone metastasis of PCa.

## Materials and Methods

### Cell lines, antibodies and reagents

Cell lines, antibodies and reagents are listed in Supplementary Table 1. Cells were tested for mycoplasma using MycoAlert™ Mycoplasma Detection Kit (LONZA, LT07-418) and authenticated using short tandem repeat.

### Adipogenesis and Chondrogenesis assays

2H11 cells treated with BMP4 and/or Palo were switched into adipocyte differentiation medium (RPMI Medium with 10% charcoal-stripped serum, 2 μg/mL insulin, 1 μM dexamethasone and 2 μM rosiglitazone) for 10 days. For chondrogenic differentiation, treated 2H11 cells were cultured in chondrogenic differentiation medium (Lonza) for 14 days. Mesenchymal stem cell line C3H10T1/2 were used as a positive control. Oil Red O staining for adipocytes was performed for 30 min on cells grown in adipocyte differentiation medium. Alcian blue staining for chondrocytes was performed on cells cultured in chondrogenic medium.

### Quantitative PCR (qRT-PCR)

Total RNA was extracted using RNeasy Mini Kit (Qiagen). cDNA was synthesized from 2 μg of total RNA using TaqMan Reverse Transcription Reagents (Life Technologies). qRT-PCR was performed using SYBR green (Applied Biosystems, CA, USA) fluorescence signals under the following PCR conditions: 40 cycles of 15-sec denaturation at 95°C and 1-min amplification at 60°C. All reactions were run in duplicates and normalized using Gapdh. The mouse-specific primer sequences are listed in Supplementary Table 2.

### Immunoblotting, immunofluorescence, and immunoprecipitation

Cell lysates (20 μg) were resolved on SDS-PAGE, and proteins bands were analyzed by immunoblotting with indicated antibody. Protein levels were quantified against loading control using ImageJ. For immunofluorescence analysis, cells were fixed and stained with primary antibodies (1:50 – 1:500) overnight, followed by Alexa-Fluor conjugated secondary

Author Manuscript Author Manuscript Author Manuscript Author Manuscript

antibodies. Images were acquired on a Nikon TE2000 widefield microscope system (27). For immunoprecipitation, nuclear fractions were isolated using lysis buffer as described (28). Lysates were incubated overnight with antibodies and the protein-antibody complexes were analyzed by western blotting.

### Mineralization assays

2H11 cells (murine lymphoid endothelial cells) were cultured in serum-free DMEM medium overnight followed by treatment with BMP4 (100 ng/mL), palovarotene (1 μM), or both in serum-free medium for 48 h, then switched into osteoblast differentiation medium (α-MEM containing 10%FBS, 100 μg/ml ascorbic acid and 5 mmol/L β-glycerophosphate) for 12-14 days with fresh medium changes every three days as described (28). MS1 (Murine pancreatic microvascular endothelial cells) and SVR (MS1 cells transfected with H-ras) were treated in 0.5% FBS DMEM medium plus BMP4, palovarotene, or both overnight, then switched into osteoblast differentiation medium for 12-14 days. HUVEC (human umbilical vein endothelial cells) primary cells (Lonza) from passage 1-4 were used for study. HUVEC cells were cultured in EGM™ Endothelial Cell Growth Medium. Confluent HUVEC cells were cultured in EGM serum-free medium overnight, and switched to HMSC Osteogenic BulletKit medium (Lonza) with BMP4 and/ or palovarotene for 14-21 days. Cells were fixed with formalin and incubated with Alizarin Red S solution or $AgNO_3$ solution (von Kossa staining) as described (4). The mineralized nodules were quantified using Image J software.

### Isolation of mouse lung endothelial cells

Mouse lung was cut into very small pieces and incubated in 2% collagenase DPBS with $Ca^{2+}$/Mg (Gibco, 17100-017). The tissues were digested at 37°C for 45 min in an incubator with constant rotation. DMEM containing 10% FBS was added to the suspension to stop the digestion. The suspension was filtered through a 70 μm cell strainer and centrifuged at 400 g at 4°C for 8 min. The pellet represents mouse lung endothelial cells (MLEC). MLECs were cultured in endothelial cell growth medium (High glucose DMED with 10% FBS, 100 μM non-essential amino acids, 100 μM sodium pyruvate, 0.1 unit/mL heparin and 100 μg/ml endothelial cell growth factor). For MLEC differentiation, MLECs were cultured in serum-free DMEM medium overnight followed by treatment with BMP4, palovarotene, or both in serum-free medium for 48 h, then switched into Stempro osteoblast differentiation medium for 14-20 days.

### Generation of C4-2b-BMP4-LT, TRAMP-BMP4-LT, and MycCaP-BMP4-LC cell lines

C4-2b-BMP4-LT cell line, expressing BMP4, luciferase reporter, and red fluorescence protein Tomato, was generated as described (4). C4-2b cells that expressed both BMP4 and Luc were selected with G418 followed with fluorescent activated cell sorting. TRAMP-BMP4 and MycCaP-BMP4 cell lines were generated by using a bicistronic retroviral vector that contains mouse BMP4 cDNA. The luciferase reporters were introduced into TRAMP-BMP4 and MycCaP-BMP4 cells using bicistronic retroviral vector pBMN-Luc-IRES-Tomato and a lentivirus vector FUW-Luc-mCh-Puro, respectively. The TRAMP-BMP4-LT or MycCaP-BMP4-LC cells that co-expressed both BMP4 and Luc were selected with puromycin (for BMP4) and FACS (for Tomato or mCherry).

Author Manuscript Author Manuscript Author Manuscript Author Manuscript

### Generation of subcutaneous tumors

Tumor cells were injected subcutaneously in male SCID mice. Mice were treated by oral gavage with palovarotene (2 mg/kg/day), ATRA (6-12 mg/kg/day) or corn oil (as control).

### Intrabone injection

TRAMP-BMP4-LT ($1x10^6$) or MycCaP-BMP4-LC ($0.5x10^6$) cells were injected into femurs of SCID mice. Palovarotene (2 mg/kg/day) or ATRA (8-12 mg/kg/day) was administered by daily oral gavage 3 days before tumor inoculation and continued throughout the treatment period. Tumor growth was monitored weekly by bioluminescent imaging (BLI). Femurs were fixed in 10% paraformaldehyde for μCT analysis using Bruker SkyScan 1276 (Bruker, Kontich, Belgium). CT Analyzer (Bruker) software (version 1.17.7.2) was used for data analyses.

### Bone mineralization analysis

Tumor sections were stained for von Kossa (silver staining) or Goldner trichrome to visualize mineralization.

### Cell proliferation analysis

Cell proliferation was determined by viable cell counting by CellTiter 96 AQueous Non-Radioactive Cell Proliferation Assay (MTS) Kit (Promega).

### Proximity ligation assays

2H11 cells cultured in serum-free DMEM medium were treated with BMP4 (100 ng/mL) for 24 h, fixed and co-incubated overnight with pairs of primary antibodies (sc, Santa Cruz; cs, Cell Signaling) as follows: anti-Smad1 (mouse sc7965, 1:50) and anti-RARγ (rabbit cs8965, 1:100); anti-Smurf1 (mouse sc-100616, 1:50) and anti-pSmad1/5 (rabbit cs9516, 1:100); anti-Smurf1 (mouse sc-100616, 1:50) and anti-RARγ (rabbit cs8965, 1:100). Proximity ligation assays were performed using DUOLink In Situ Red Starter Kit (DUO92101) (Sigma) with anti-Mouse MINUS (DUO92004) and anti-Rabbit PLUS (DUO92002) PLA probes as previously described (27). Incubations with a single antibody or no antibody were used as negative PLA controls. PLA images were acquired on a Nikon TE-2000 confocal microscope and analyzed using NIS-Elements 5.21.02 software (Nikon) (27).

### RNAseq analysis

2H11 cells were treated with BMP4 (100 ng/mL) with or without palovarotene (1 uM) in serum-free medium for 48 h. Total RNA was extracted using RNeasy Mini Kit (Qiagen) and prepared for RNAseq analysis at Arraystar Inc. (Rockville, MD). Transcriptome data have been deposited at GSE168157.

### Knockdown of RARα, RARβ or RARγ in 2H11 cells

RARα, RARβ, RARγ or Smurf1 in 2H11 cells were knocked down using MISSION pLKO.1 lentiviral shRNA (MilliPORE Sigma). shRNA clones were selected with 5 μg/mL puromycin. Cells infected with empty pLKO.1 lentiviral vector were used as controls. Primers for shRNA are listed (Supplementary Table 2).

Author Manuscript Author Manuscript Author Manuscript Author Manuscript

### Treatment of MDA PCa-118b tumors with ATRA in vivo

MDA PCa-118b PDX was maintained by serial passage in SCID mice as described (3). MDA PCa-118b ($1x10^6$) were injected into SCID mice subcutaneously. After 3 weeks, mice bearing MDA PCa-118b tumors were grouped into two groups based on similar tumor size. ATRA (6-12 mg/kg/day) was administered through oral gavage daily 6 days per week. Control mice were administered with corn oil. Tumor sizes were measured by caliper.

### Enzyme-linked immunosorbent assay (ELISA)

Tenascin C protein level was determined using mouse Tenascin C ELISA Kit (NBP2-78767; Novus Biological Inc). Serum samples from mice bearing MycCaP-BMP4 tumor treated with or without ATRA or palovarotene were diluted in PBS and used in ELISA.

### Bone histomorphometry analysis

Bone histomorphometry analysis on non-decalcified mouse femurs was performed by M.D. Anderson Cancer Center Bone Histomorphometry Core Laboratory as described (29). Femurs were sectioned at 5 μm thickness in a longitudinal plane. The measurement area excluded the 150 μm area adjacent to the cortical bone. For each sample, measurements for OSBs and osteoclasts were performed on 2 separate 5 μm thick Toluidine Blue and TRAP stained sections, respectively. Blood vessel quantification was performed on one Toluidine Blue stained 5 μm thick bone section.

### Isolation of mouse adipocyte stem cells

To isolate mouse adipocyte stem cells (mADSCs), adipose tissues were collected from 8-week-old mice and cut into small pieces. Collagenase (0.2%) was added and adipose tissues were incubated at 37°C for 1 h. DMEM containing 10% FBS was added to the suspension and centrifuged at 1200 rpm for 5 min. mADSCs at the bottom of the tube were isolated and cultured in adipocyte differentiation medium or osteoblast differentiation medium.

### Matrigel Tube formation assay

Basement Membrane Matrix (356260, Corning) was added to a 48-well plate (100 μL/well) and incubated for 12 h at 37°C for solidification. 2H11 cells ($2 \times 10^4$) were added to the Matrigel with or without various concentrations of palovarotene. Cells treated with 0.1 μM cabozantinib was used as a positive control. Tube formation was observed at 0 or 20 h following transfer to Matrigel and quantified by detecting the nodes in four randomly chosen fields.

### Immunohistochemistry of CD31 expression in tumors

Formalin-fixed, paraffin-embedded C4-2b or MycCaP tumors were generated by injecting C4-2b or MycCaP cells subcutaneously into SCID mice treated with or without ATRA. The tumor sections were incubated with anti-CD31 antibody overnight at 4°C, followed with HRP-conjugated secondary antibodies. Images were scanned and analyzed by Aperio ImageScope software.

Author Manuscript Author Manuscript Author Manuscript Author Manuscript

### Study approval

Animal studies have been approved by the Institutional Animal Care and Use Committee at M.D. Anderson Cancer Center.

### Statistical analysis

Data were expressed as the mean ± S.D. P value was computed by two-sided t-test. $p < 0.05$ by Student's *t*-test was considered statistically significant.

### Data availability

Materials (plasmids) generated in this study will be made available upon reasonable request to the lead contact. Their delivery could require a material transfer agreement. The sequencing data generated from this study are publicly available in Gene Expression Omnibus (GEO; RRID:SCR_005012) at GSE168157 and GSE168321.

## Results

### RARγ agonist palovarotene inhibits EC-to-OSB transition

We employed 2H11 cells, a murine lymphoid EC line (30), for our EC-to-OSB transition studies. As 2H11 cells also express CD34 (30), a stem cell marker, we evaluated whether 2H11 cells possess multilineage differentiation potential beyond OSBs. We observed that 2H11 cells cannot be differentiated into chondrocytes or adipocytes (Supplementary Fig. 1A, B), when compared with the pluripotent stem cell line C3H10T1/2 that differentiated into chondrocytes or adipocytes under the same culturing conditions (Supplementary Fig. 1A, B). We found that 2H11 ECs can be induced to undergo EC-to-OSB transition by treating with BMP4 (100 ng/mL) for 48 h, based on the expression of OSX, an osteoblast cell fate determination factor, and osteocalcin (Fig. 1A, B). Addition of Palo significantly inhibited BMP4-induced EC-to-OSB transition as shown by the inhibition of OSX and osteocalcin expression (Fig. 1A, B), and osteoblast mineralization, as indicated by Alizarin Red (Fig. 1C) and von Kossa staining (Fig. 1D), compared to BMP4 alone when cultured in osteoblast differentiation medium for 21 days. Without BMP4, Palo alone had no effect on EC-to-OSB transition. These results suggest that Palo inhibits BMP4-induced EC-to-OSB transition.

### Inhibition by palovarotene occurs in the early stages of EC-to-OSB transition

Upon BMP4 treatment, 2H11 cells first transition into OSB by day 2 (days 0-2, Transition Phase). EC-OSB hybrid cells then undergo OSB differentiation and express bone matrix proteins (days 3-14, Differentiation Phase), and finally mineralize by day 20 (Mineralization Phase) (Fig. 1E). To examine whether Palo could inhibit BMP4-induced bone formation after EC-to-OSB transition has already been initiated, Palo was added to cells at different transition stages. Palo was most effective during early transition (D0 – D2), reaching ~80 – 90% inhibition of BMP4-stimulated activities (Fig. 1G, 1I). Palo still inhibited OSX (Fig. 1F) and osteocalcin expression (Fig. 1H), albeit with decreasing efficacy when added to the cultures on D2, D5, D8, or D11 (Fig. 1F-1I). Similarly, inhibition of mineralization was also most effective during early transition and less effective when Palo was added in later

Author Manuscript Author Manuscript Author Manuscript Author Manuscript

phases of EC-to-OSB transition (Fig. 1J and 1K). These observations suggest that Palo is most effective in inhibiting early stages of BMP4-induced EC-to-OSB transition.

To assess whether other ECs can also undergo transition into OSBs, we treated primary mouse lung ECs (MLEC), MS-1 cells (a murine pancreatic microvascular EC line), SVR cells (an H-ras transfected MS-1 cell line) (31), and primary human umbilical vein ECs (HUVEC) with BMP4 and cultured the cells in osteogenic medium. We found that all of these ECs can be induced to become OSBs by BMP4 as evidenced by an increase in Alizarin Red staining (Supplementary Fig. 1C-F). Addition of Palo significantly inhibited BMP4-induced EC-to-OSB transition as indicated by the inhibition of Alizarin Red staining (Supplementary Fig. 1C-F). These results suggest that BMP4 can induce EC-to-OSB transition in ECs derived from several organs and that Palo can inhibit this BMP4-induced EC-to-OSB transition.

## Palovarotene reduces PCa-induced aberrant bone formation in xenograft animal models

We employed three osteogenic xenograft models to examine Palo effects on PCa-induced bone formation. In the first model, C4-2b-BMP4 cells, which form osteogenic tumors (4), were injected subcutaneously into SCID mice (Fig. 2A). Mice were treated with or without Palo (2 mg/kg/day) by oral gavage. Palo significantly reduced tumor-induced bone formation compared to those in vehicle-treated control tumors, as determined by Goldner's Trichrome staining (Fig. 2B). Palo also led to a moderate decrease in tumor sizes compared with controls, as determined by bioluminescence imaging (Fig. 2C) and tumor weight (Fig. 2D). However, Palo did not affect C4-2b-BMP4 cell proliferation *in vitro* (Supplementary Fig. 2A) or mouse body weight (Supplementary Fig. 2B). These observations suggest that Palo reduces tumor-induced bone formation and tumor size, consistent with previous observation that PCa-induced bone supports prostate tumor growth (3,9).

In a second model, we injected osteogenic TRAMP-BMP4 cells intrafemorally into SCID mice and treated these tumor-bearing mice with or without Palo (Fig. 2E). TRAMP-BMP4 cells, generated by BMP4-cDNA transfection into TRAMP-C2 cells (32), express high levels of BMP4 protein (Supplementary Fig. 2C). TRAMP-BMP4 increased the bone mineral density of the tumor-bearing femurs (Fig. 2F, left), and induced bone formation in the bone marrow (Fig. 2F, middle) compared to control un-injected legs. Palo significantly reduced the bone mineral density in the tumor-bearing femurs compared with those in non-treated mice (Fig. 2F, right), and moderately decreased PCa growth in bone at week 4, although the decrease did not reach statistical significance (Fig. 2G). Palo did not affect TRAMP-BMP4 cell proliferation *in vitro* (Supplementary Fig. 2D). In this experiment, Palo led to a small decrease in mouse body weight compared to untreated mice (Supplementary Fig. 2E). These results suggest that Palo reduces TRAMP-BMP4-induced bone formation in mouse femurs.

In a third model, MycCaP-BMP4 cells were injected intrafemorally into SCID mice and treated with or without Palo (Fig. 2H). MycCaP-BMP4 cells, generated by BMP4-cDNA transfection into MycCaP cells that were derived from prostate tumor of Hi-Myc mice (33), express a high level of BMP4 protein (Supplementary Fig. 2F). X-Ray analysis showed that MycCaP-BMP4 in femurs induced an osteoblastic bone response in tumor-bearing femurs,

Author Manuscript Author Manuscript Author Manuscript Author Manuscript

and Palo significantly reduced this response (Fig. 2H). Palo also exhibited a trend towards reduced tumor growth (Fig. 2I). Palo did not affect MycCaP-BMP4 cell proliferation *in vitro* (Supplementary Fig. 2G) and mouse body weight (Supplementary Fig. 2H). Together, the combined results from these three osteogenic xenograft models suggest that Palo reduces PCa-induced bone formation accompanied with a trend of decreased tumor growth.

## Palovarotene reduces BMP4-stimulated pSmad1 levels in pSmad1/RARγ complex

Smad1 phosphorylation is one of the downstream BMP4 signaling pathways in 2H11 cells (28). pSmad1 levels were significantly increased by BMP4, and Palo reduced BMP4-stimulated pSmad1 levels (Fig. 3A). Total Smad1 was also increased by BMP4 and slightly decreased by Palo (Fig. 3A). BMP4 also increased nuclear localization of pSmad1, which was decreased by Palo (Fig. 3B). Similar patterns of distribution were observed with Smad1 (Fig. 3B). In contrast, total and nuclear RARγ levels were not affected by BMP4 or Palo (Fig. 3A, B). These observations suggest that Palo leads to a decrease in BMP4-stimulated nuclear pSmad1 levels.

Using nuclear extracts, we showed that immunoprecipitation of RARγ pulled down pSmad1, while the reciprocal immunoprecipitation of Smad1 pulled down RARγ (Fig. 3C), suggesting that pSmad1 forms a complex with RARγ in BMP4-treated 2H11 cells. Further, *in situ* proximity ligation assay (PLA) for the potential physical association between pSmad1 and RARγ showed a significant increase in PLA signals, visualized as individual fluorescent spots, in the nucleus of BMP4-treated 2H11 cells but not in control cells (Fig. 3D). No PLA signals were observed in BMP4-treated cells incubated with a single antibody alone as controls (Fig. 3D). Palo was found to reduce BMP4-mediated nuclear pSmad1/RARγ complex formation by both co-immunoprecipitation (Fig. 3C) and PLA (Fig. 3D). These results suggest that Palo inhibits BMP4-stimulated pSmad1/RARγ nuclear complex formation.

## Palovarotene increases Smurf1-mediated phospho-Smad1 degradation

We postulated that Palo inhibits BMP4-stimulated pSmad1/RARγ nuclear complex formation by enhancing its degradation via Smad ubiquitination regulatory factor1 (Smurf1) (34). Indeed, Palo led to the recruitment of E3-ubiquitin ligase Smurf1 to the nuclear pSmad1/RARγ complex (Fig. 3E). Further, PLA showed a significant increase in Smurf1 association with pSmad1 (Fig. 3F) as well as Smurf1 association with RARγ (Fig. 3G), only in the presence of RAR activation by Palo. Together, these observations suggest that Palo recruits Smurf1 to the nuclear RARγ/pSmad1 complex.

We knocked down Smurf1 and found an increase in pSmad1 levels in 2H11-shSmurf1#1 and #2 clones compared to vector control (Fig. 3H), consistent with a role of Smurf1 in regulating pSmad1 levels. In 2H11-shSmurf1 clones, Palo-mediated decrease in pSmad1 was abrogated compared with vector controls (Fig. 3I), suggesting that Palo mediates pSmad1 degradation through Smurf1, likely through pSmad1 ubiquitination for proteasomal degradation. Together, our studies suggest that RAR activation by Palo causes BMP4-stimulated pSmad1 degradation by recruiting Smurf1 into the nuclear pSmad1/RARγ complex (Fig. 3J).

Author Manuscript Author Manuscript Author Manuscript Author Manuscript

### Palovarotene alters the BMP4-induced transcriptome

We characterized the Palo-regulated transcriptome by RNAseq. RNAseq analysis showed that mRNA levels of 591 genes were upregulated more than 1.5-fold by BMP4 when compared to 2H11 cells (2H11-BMP4 vs 2H11) (Fig. 4A) (see GSE168321). By using fold enrichment to select for the top 215 pathways followed with lowest false discovery rate, pathway analysis showed that regulation of osteoblast differentiation, bone morphogenesis and bone mineralization were the most significantly upregulated pathways by BMP4 (Fig. 4B), consistent with ECs transition into OSBs. Upon Palo treatment for 48 h, mRNA levels of 756 genes were downregulated compared to BMP-treated sample ([BMP4+Palo] vs BMP4) (Fig. 4A) (see GSE168157). Pathway analysis showed that genes involved in regulation of ossification were most significantly downregulated by Palo (Fig. 4C), consistent with an effect of Palo on inhibiting bone formation.

We identified 146 transcripts that were upregulated by BMP4 and downregulated by Palo (Fig. 4A). Pathway analysis showed that these 146 transcripts are enriched in genes involved in regulation of epithelial to mesenchymal transition and the function of osteoblasts, osteoclasts and chondrocytes in Rheumatoid Arthritis (Fig. 4D), consistent with a role of Palo in inhibiting EC-to-OSB transition. Further, we found that 8 transcription factors that play critical roles in cell fate change, including Slug, Foxo1, and Id4, were downregulated by Palo (Fig. 4E). Indeed, mRNAs of these transcription factors were upregulated by BMP4 and downregulated by Palo (Fig. 4E). Slug, also known as Snai2, is a cell fate determinant (35). Foxo1 regulates osteoblast numbers, bone mass, and the differentiation of mesenchymal cells into osteoblasts (36). Id4 is a DNA-binding protein that is a downstream effector of BMP signaling and regulates various cellular processes (37). Because the expression of Id proteins (Id1, Id2, Id3, and Id4) has been reported to be regulated by BMPs (38,39), we further examined the expression of all 4 Ids in 2H11 cells. Our RNAseq analysis showed that only Id1 and Id4, but not Id2 and Id3, expression was downregulated by Palo (Supplementary Fig. 3A). qRT-PCR analysis showed that while all four Ids were upregulated by BMP4 during EC-to-OSB transition, only Id1 and Id4, but not Id2 and Id3, were downregulated by Palo (Supplementary Fig. 3B), consistent with the RNAseq analysis (Supplementary Fig. 3A). The differential effects of Palo on BMP4-induced Id expression and whether Id1 and Id4 are involved in EC-to-OSB transition require further investigation. These results suggest that the binding of Palo to RARγ alters Smad1 signaling, leading to transcriptional changes of several cell fate-related transcription factors involved in osteoblastogenesis.

We also identified 39 secreted proteins upregulated by BMP4 and downregulated by Palo (Fig. 4F and Supplementary Table 3). These proteins, including growth factors, cytokines, proteases, and bone matrix proteins (Fig. 4G and Supplementary Table 3), collectively termed “osteocrines” (12), may be involved in stromal-PCa communication critical for PCa progression in bone. The mRNA levels of Fgf10, Tslp, Mgp and Tnc were upregulated by BMP4 and significantly downregulated by Palo in 2H11 cells (Fig. 4H). Fgf10 is required for limb and lung development (40,41). Tenascin C (TNC), a bone matrix protein, plays a role in inducing stemness and increasing metastatic potential of tumor cells (42). Thymic stromal lymphopoietin (TSLP), a Th2 cytokine, is involved in the induction and progression

Author Manuscript Author Manuscript Author Manuscript Author Manuscript

of various tumors (43). These “osteocrines” may be involved in Palo-mediated inhibition of tumor growth and can be used as serum biomarkers for monitoring response to Palo treatment.

## RARα and RARβ are also involved in EC-to-OSB transition

RAR family proteins contain 3 isoforms, RARα, RARβ and RARγ. Palo is a synthetic retinoic acid that has a high affinity for RARγ. Whether RARα and/or RARβ are involved in EC-to-OSB transition is not clear. We determined that 2H11 cells express all three isoforms (Fig. 5A-C). Knockdown of RARα, β, or γ (Fig. 5A-C) significantly reduced BMP4-induced osteocalcin expression in 2H11-shRARα, β and γ clones (Fig. 5A-C). Thus, all three RAR isoforms are involved in BMP4-induced EC-to-OSB transition. Knockdown of RAR isoforms also led to an inhibition of BMP4-induced pSmad1 levels (Fig. 5D), suggesting similar mechanisms of inhibition mediated by the three RAR isoforms.

## ATRA and 13-cis-retinoic acid inhibit EC-to-OSB transition

We next examined if retinoic acids with broad spectrum for RAR isoforms can also inhibit BMP4-induced EC-to-OSB transition. We found that tretinoin (ATRA) and isotretinoin (13-cis-RA), pan-RAR agonists used in the clinic (44), both inhibited EC-to-OSB transition in a dose-dependent manner (Fig. 5E-G), to a similar extent as that of Palo. ATRA and 13-cis-RA also inhibited BMP4-induced nuclear pSmad1 to levels similar as that by Palo (Fig. 5H). Thus, RAR agonists, including Palo, ATRA and 13-cis-RA, can inhibit BMP4-induced EC-to-OSB transition.

## ATRA inhibits BMP4-induced bone formation following castration

In an initial study, ATRA was found to reduce MycCaP-BMP4 tumor growth (Supplementary Fig. 4A), with a trend of reduced bone mineral density (BMD), percent bone volume (BV/TV) and bone surface density (BS/TV) compared to control non-treated mice (Supplementary Fig. 4B). However, ATRA (12 mg/kg) led to a significant decrease in body weight (Supplementary Fig. 4C). Dose reduction to 6 mg/kg (Supplementary Fig. 4A, arrow) alleviated toxicity but also lessened the tumor response (Supplementary Fig. 4A). Thus, the study was repeated with modifications (Fig. 6A). Mice were inoculated subQ+intrafemur with MycCaP-BMP4 cells and one group received ATRA (10 mg/kg) and the other received vehicle. After one week, both groups were castrated (Fig. 6A, red arrow). Castration led to a temporary halt or decrease of tumor growth in both control and ATRA-treated mice, after which tumor growth resumed in both groups, and tumor growth was reduced by ATRA (Fig. 6A). Subcutaneous MycCaP-BMP4 tumors exhibited ectopic bone formation (Fig. 6B), similar to those observed with C4-2b-BMP4 tumors (Fig. 2A). ATRA reduced MycCaP-BMP4-induced bone formation measured by μCT and von Kossa staining (Fig. 6B).

In the MycCaP-BMP4 tumor-bearing femurs, ATRA led to a trend of decreases in BMD, BV/TV, BS/TV, and trabecular bone density (Tb.N) in the tumor-bearing femurs compared with those in control mice (Fig. 6C), although some parameters did not reach statistical significance. ATRA did not affect MycCaP-BMP4 cell proliferation (Supplementary Fig. 4D), as also observed with Palo (Supplementary Fig. 2G). A small decrease in body weight

Author Manuscript Author Manuscript Author Manuscript Author Manuscript

was observed at day 28 (Supplementary Fig. 4E). Together, these results suggest that ATRA reduces MycCaP-BMP4-induced bone formation and tumor growth in mice undergoing castration.

### ATRA inhibits MDA PCa-118b bone formation

MDA PCa-118b expresses BMP4 endogenously and generates bone-forming tumors when implanted subcutaneously (3). In MDA PCa-118b PDX model, due to significant variation in tumor sizes, ATRA treatment was initiated after 3 weeks, when tumors have reached measurable sizes. We found that ATRA also reduced bone formation and tumor growth of the MDA PCa-118b xenograft (Fig. 6D, E). In addition, we also repeated the MDA-PCa-118b studies using longer treatment times. After tumors were grown for 3 weeks, tumors that reached the size of 35 $mm^3$ were randomized for ATRA treatment (Supplementary Fig. 5A). Tumors in the control mice grew fast and reached large tumor sizes after 18 days. However, tumors in the ATRA-treated mice grew slower and the treatment was continued for an additional 21 days (Supplementary Fig. 5B-D). Together, these results suggest that ATRA not only inhibits MDA PCa-118b bone formation but also reduces the growth of pre-formed PCa tumor.

### Palovarotene or ATRA reduces plasma Tenascin C levels

In preparation for using Palo or ATRA to reduce tumor-induced bone formation in patients with castrate-resistant osteoblastic bone metastasis, we examined TNC levels, which was increased during EC-to-OSB transition (Fig. 4H) (45), in the plasma of SCID mice with intrafemur MycCaP-BMP4 tumors treated with or without ATRA or Palo. Both ATRA and Palo significantly reduced plasma TNC levels compared to untreated controls, as quantified by ELISA (Fig. 6F), consistent with inhibition of EC-to-OSB transition by ATRA or Palo. These results suggest that plasma TNC levels could be used to monitor response to treatments.

### ATRA does not lead to overall bone loss in non-tumor containing bones

We also examined whether ATRA leads to unwanted bone loss in healthy non-tumor-bearing bones. Bone histomorphometry analyses of contralateral non-tumor containing femurs from MycCaP-BMP4 castration plus ATRA-treated animals (Fig. 6C) showed that there were no significant changes in several bone parameters compared to control castrated mice (Fig. 6G). Similarly, no consistent changes on parameters related to activities of osteoblasts and osteoclasts (Supplementary Fig. 6A, B) were observed. Our previous study showed that castration reduced bone volume and an increase in osteoclast density (46). These results suggest that ATRA does not further worsen the osteoporotic effects from castration.

## Discussion

Our studies identify a strategy to target PCa-induced bone formation to interfere with the cross-talk between stromal components and metastatic PCa tumor cells. We show that activation of RAR by agonists, including Palo and ATRA, inhibits stromal reprogramming through blocking BMP4-induced EC-to-OSB transition and reduces PCa-induced aberrant bone formation and tumor growth *in vivo* (Fig. 6H). We also show that Palo and ATRA

Author Manuscript Author Manuscript Author Manuscript Author Manuscript

inhibit EC-to-OSB transition through a non-canonical RAR pathway (Fig. 6H). Because PCa-induced aberrant bone formation enhances PCa progression (3) and also resistance to therapy (12), our studies suggest that Palo or ATRA may be used to reduce tumor-induced bone formation to improve therapy outcomes for patients with PCa bone metastasis. Presently, effective therapies directed at blocking mechanisms of PCa bone metastasis are limited. Palo is currently being evaluated for its potential to reduce heterotopic (extra-skeletal) ossification for the rare genetic disease FOP (47). ATRA and 13-cis-RA have previously been used for the treatment of PCa with limited or no efficacy (48). However, the potential to "repurpose" these agents to target tumor-induced bone in the treatment of bone metastatic PCa has not been explored. We also propose to use a new generation retinoid acid agonist, palovarotene, which has a more stable pharmacokinetic profile and does not appear to induce CYP26 enzymes, allowing more predictable dosing regimens (for review, see Hind and Stinchcombe (49)). Palo was shown to be safe for long-term treatments (47), making its combination with other cancer-targeted therapies for PCa bone metastasis promising. Our studies thus identify a novel therapy strategy that targets tumor-induced stromal reprogramming as treatment for PCa bone metastasis.

Our previous discovery that osteoblastic bone lesions arise from EC-to-OSB transition (4) led us to hypothesize that inhibiting this transition would represent a novel therapy strategy for bone-metastatic PCa. The current study credentials the EC-to-OSB transition as a valid therapy target. This occurred without significant effect on non-tumor involved healthy bone in castrated mice as measured by bone histomorphometry. The fact that plasma levels of TNC correlated with ATRA's effect on EC-to-OSB transition suggests their potential use as a blood-based biomarker to monitor response to ATRA treatment (Fig. 6H). Together, our studies provide a framework for the clinical development of ATRA or Palo for the treatment of bone metastatic PCa.

Although RARs are nuclear transcription factors, our study suggests that activation of RARs by Palo or ATRA inhibits EC-to-OSB transition via a non-canonical RAR pathway. We found that RARs form a complex with pSmad1 during BMP4-stimulated EC-to-OSB transition. It is possible that the formation of RAR/pSmad1 complex prevents the degradation of pSmad1 by Smurf1. Upon retinoic acid treatment, Smurf1 is recruited to the pSmad1/RAR/ligand complex to degrade pSmad1 (Fig. 6H). Our studies likely reveal a novel mechanism for retinoic acids' effects on modulating skeletal development (22-24). Future studies should determine whether RARs signal through other yet-to-be identified pathways in different cellular contexts.

While we showed that ECs are one source of the tumor-induced bone (4), several cell populations with osteogenic capacity have also been described in the bone marrow, including NG2+ pericytes (50), LepR+ cells (51,52), and Gli1+ cells (53). Although lineage tracing studies allowed us to follow OSBs that are derived from endothelial precursors (4), it is not feasible in this model to establish the fraction of OSBs that are contributed from endothelial source in the total OSBs. Thus, the possibility that other progenitor cells may be recruited and contribute to aberrant bone formation in PCa bone metastasis cannot be excluded. Strategies that can distinguish OSBs from different progenitor sources are needed to address this intriguing question.

Author Manuscript Author Manuscript Author Manuscript Author Manuscript

Adipocyte stem cells have been reported to differentiate into OSBs when cultured in osteogenic medium (54,55)(Supplemental Fig. 7A). We examined whether Palo can inhibit adipocyte-to-OSB transition. In contrast to Palo's inhibitory effect on EC-to-OSB transition, we found that Palo alone can enhance adipocyte-to-OSB transition (Supplemental Fig. 7B), consistent with the report by others (55,56), and Palo did not inhibit BMP4-induced adipocyte-to-OSB transition (Supplementary Fig. 7B). Thus, Palo-mediated decrease in EC-to-OSB transition and bone formation is unlikely to be due to an inhibition of adipocyte-to-OSB transition.

Our finding that Palo or ATRA decreases tumor volumes raises the question of whether RAR agonists are exerting a direct effect on tumor cells or an indirect effect through inhibition of tumor-induced bone. Others have shown that RAR agonists are not very effective in inducing growth arrest in PCa cell lines *in vitro*, as high concentrations (~1–10 μM) are generally needed (57-59), in agreement with our results that Palo or ATRA does not inhibit proliferation of C4-2b-BMP4, TRAMP-BMP4, and MycCaP-BMP4 cells (Supplementary Fig. 2A, D, G). Given that ATRA has been reported to inhibit angiogenesis in acute promyelocytic leukemia (60) and our bone histomorphometry analysis showed ATRA has effects on several EC parameters (Supplementary Fig. 6C), we examined whether Palo has an effect on EC proliferation and tube formation *in vitro*. We found that Palo moderately inhibited the proliferation of 2H11, MS1, and SVR cells (Supplementary Fig. 8A). Palo also inhibited EC tube formation of HUVEC, 2H11, MS1, and SVR cells (Supplementary Fig. 8B). When tested *in vivo* on subcutaneously generated non-osteogenic MycCaP, C4-2b and TRAMP-C2 tumors, ATRA causes a small decrease of tumor volumes (Supplementary Fig. 8C). We also examined ATRA treatment on tumor microvessel density using CD31 staining (Supplementary Fig. 8D). We found that the microvessel density of MycCaP and C4-2b tumors was moderately inhibited by ATRA treatment. Together, these results suggest that ATRA has an effect on angiogenesis. Because our previous studies showed that reduction of bone formation resulted in a decrease of tumor-induced bone formation in a genetic mouse model and a xenograft model (3,4), these observations suggest that ATRA or Palo's effects on inhibiting osteogenic tumors are likely due to both a reduction in tumor-induced bone formation and inhibition of tumor angiogenesis.

We note that ATRA or Palo's effects on bone-forming tumor growth are moderate. Thus, we posit that ATRA or Palo in combinations with epithelial-targeting therapies (e.g. docetaxel) will be more effective for tumor growth inhibition. As we previously showed that tumor-induced bone is one source of therapy resistance (12), it is possible that Palo or ATRA, by reducing tumor-induced bone formation, will reduce resistance to therapies. Such an application requires further investigation.

Although Palo has been reported to be an RARγ-specific agonist in the literature (18,49) and several clinical trials were performed based on such a property (NCT 02190747, NCT 03312634, NCT 02279095, NCT03442985), the binding affinities of Palo to the three RAR isoforms have not been published. However, the binding affinities of Compound 7, which shares a close structural identity with Palo (Supplementary Fig. 8E), as reported in US patent No. 6777418 are 260 nM, 140 nM, 17 nM for purified RARα, β, γ proteins, respectively,

Author Manuscript Author Manuscript Author Manuscript Author Manuscript

suggesting that Palo may be more potent for RARγ than RARα or RARβ isoforms by about 15 and 8-fold, respectively.

With the advancement of immune therapies, performing the experiments in immunocompetent mice would yield information on the impact of immune infiltrates in the context of increased bone-formation and retinoic acid signaling. Engblom et al. (61) reported that OSBs supply cancer-promoting neutrophils to modulate the immune system in lung cancer. Retinoic acid and retinoic acid receptors are modulators of the immune system (62). Thus, it is possible that both tumor-induced bone formation and Palo have an impact on immune responses. Establishing syngeneic mouse tumor models will allow us to determine whether the proposed therapy approach is also effective in immunocompetent mouse. Such an approach is currently being developed.

In conclusion, we found that activation of RARs by agonists, including Palo and ATRA, targets the molecular basis of PCa-induced aberrant bone formation, and Palo and ATRA are promising therapeutic agents for the treatment of PCa bone metastasis.

## Supplementary Material

Refer to Web version on PubMed Central for supplementary material.

## Acknowledgements

This work was supported by grants from the NIH RO1 CA174798 (to SHL and LYYL), P50 CA140388 (to CJL, SHL), P30 CA016672, Cancer Prevention and Research Institute of Texas CPRIT RP150179 and RP190252 (to SHL and LYYL), and the Biology of Inflammation Center Arthritis Research Endowment AR00108 (to LYYL).

## References

1. Ye XC, Choueiri M, Tu SM, Lin SH. Biology and clinical management of prostate cancer bone metastasis. Front Biosci 2007;12:3273–86 [PubMed: 17485298]
2. Logothetis CJ, Lin SH. Osteoblasts in prostate cancer metastasis to bone. Nature reviews Cancer 2005;5:21–8 [PubMed: 15630412]
3. Lee YC, Cheng CJ, Bilen MA, Lu JF, Satcher RL, Yu-Lee LY, et al. BMP4 Promotes Prostate Tumor Growth in Bone through Osteogenesis. Cancer Res 2011;71:5194–203 [PubMed: 21670081]
4. Lin SC, Lee YC, Yu G, Cheng CJ, Zhou X, Chu K, et al. Endothelial-to-Osteoblast Conversion Generates Osteoblastic Metastasis of Prostate Cancer. Developmental cell 2017;41:467–80 e3 [PubMed: 28586644]
5. Nordstrand A, Bovinder Ylitalo E, Thysell E, Jernberg E, Crnalic S, Widmark A, et al. Bone Cell Activity in Clinical Prostate Cancer Bone Metastasis and Its Inverse Relation to Tumor Cell Androgen Receptor Activity. Int J Mol Sci 2018;19
6. Dai J, Keller J, Zhang J, Lu Y, Yao Z, Keller ET. Bone morphogenetic protein-6 promotes osteoblastic prostate cancer bone metastases through a dual mechanism. Cancer Res 2005;65:8274–85. [PubMed: 16166304]
7. Morrissey C, Brown LG, Pitts TE, Vessella RL, Corey E. Bone morphogenetic protein 7 is expressed in prostate cancer metastases and its effects on prostate tumor cells depend on cell phenotype and the tumor microenvironment. Neoplasia 2010;12:192–205 [PubMed: 20126477]
8. Dai J, Hall CL, Escara-Wilke J, Mizokami A, Keller JM, Keller ET. Prostate cancer induces bone metastasis through Wnt-induced bone morphogenetic protein-dependent and independent mechanisms. Cancer Res 2008;68:5785–94 [PubMed: 18632632]

Author Manuscript Author Manuscript Author Manuscript Author Manuscript


9. Dai J, Keller J, Zhang J, Lu Y, Yao Z, Keller ET. Bone morphogenetic protein-6 promotes osteoblastic prostate cancer bone metastases through a dual mechanism. Cancer research 2005;65:8274–85 [PubMed: 16166304]
10. Montesano T, Giacomobono S, Acqualagna G, Colandrea M, Di Nicola A, Travascio L, et al. Our experience on pain palliation of bone metastasis with Sr-89 or Sm-153 in cancer patients resistant to a conventional analgesic therapy. A retrospective study. Clin Ter 2009;160:193–9 [PubMed: 19756320]
11. Parker C, Nilsson S, Heinrich D, Helle SI, O'Sullivan JM, Fossa SD, et al. Alpha emitter radium-223 and survival in metastatic prostate cancer. The New England journal of medicine 2013;369:213–23 [PubMed: 23863050]
12. Lee YC, Lin SC, Yu G, Cheng CJ, Liu B, Liu HC, et al. Identification of Bone-Derived Factors Conferring De Novo Therapeutic Resistance in Metastatic Prostate Cancer. Cancer Res 2015;75:4949–59 [PubMed: 26530902]
13. Medici D, Shore EM, Lounev VY, Kaplan FS, Kalluri R, Olsen BR. Conversion of vascular endothelial cells into multipotent stem-like cells. Nat Med 2010;16:1400–6 [PubMed: 21102460]
14. Horwitz EM. Building bone from blood vessels. Nat Med 2010;16:1373–4 [PubMed: 21135844]
15. van Dinther M, Visser N, de Gorter DJ, Doorn J, Goumans MJ, de Boer J, et al. ALK2 R206H mutation linked to fibrodysplasia ossificans progressiva confers constitutive activity to the BMP type I receptor and sensitizes mesenchymal cells to BMP-induced osteoblast differentiation and bone formation. J Bone Miner Res 2010;25:1208–15 [PubMed: 19929436]
16. Shore EM, Xu M, Feldman GJ, Fenstermacher DA, Cho TJ, Choi IH, et al. A recurrent mutation in the BMP type I receptor ACVR1 causes inherited and sporadic fibrodysplasia ossificans progressiva. Nature genetics 2006;38:525–7 [PubMed: 16642017]
17. Kaplan J, Kaplan FS, Shore EM. Restoration of normal BMP signaling levels and osteogenic differentiation in FOP mesenchymal progenitor cells by mutant allele-specific targeting. Gene Ther 2012;19:786–90 [PubMed: 22011642]
18. Shimono K, Tung WE, Macolino C, Chi AH, Didizian JH, Mundy C, et al. Potent inhibition of heterotopic ossification by nuclear retinoic acid receptor-gamma agonists. Nat Med 2011;17:454–60 [PubMed: 21460849]
19. Pacifici M Retinoid roles and action in skeletal development and growth provide the rationale for an ongoing heterotopic ossification prevention trial. Bone 2018;109:267–75 [PubMed: 28826842]
20. Glass CK, Rosenfeld MG. The coregulator exchange in transcriptional functions of nuclear receptors. Genes Dev 2000;14:121–41 [PubMed: 10652267]
21. Moras D, Gronemeyer H. The nuclear receptor ligand-binding domain: structure and function. Curr Opin Cell Biol 1998;10:384–91 [PubMed: 9640540]
22. Pacifici M, Cossu G, Molinaro M, Tato F. Vitamin A inhibits chondrogenesis but not myogenesis. Exp Cell Res 1980;129:469–74 [PubMed: 7428831]
23. Hoffman LM, Garcha K, Karamboulas K, Cowan MF, Drysdale LM, Horton WA, et al. BMP action in skeletogenesis involves attenuation of retinoid signaling. J Cell Biol 2006;174:101–13 [PubMed: 16818722]
24. Weston AD, Chandraratna RA, Torchia J, Underhill TM. Requirement for RAR-mediated gene repression in skeletal progenitor differentiation. J Cell Biol 2002;158:39–51 [PubMed: 12105181]
25. Cash DE, Bock CB, Schughart K, Linney E, Underhill TM. Retinoic acid receptor alpha function in vertebrate limb skeletogenesis: a modulator of chondrogenesis. J Cell Biol 1997;136:445–57 [PubMed: 9015314]
26. Weston AD, Rosen V, Chandraratna RA, Underhill TM. Regulation of skeletal progenitor differentiation by the BMP and retinoid signaling pathways. J Cell Biol 2000;148:679–90 [PubMed: 10684250]
27. Yu-Lee LY, Yu G, Lee YC, Lin SC, Pan J, Pan T, et al. Osteoblast-Secreted Factors Mediate Dormancy of Metastatic Prostate Cancer in the Bone via Activation of the TGFbetaRIII-p38MAPK-pS249/T252RB Pathway. Cancer Res 2018;78:2911–24 [PubMed: 29514796]
28. Yu G, Shen P, Lee YC, Pan J, Song JH, Pan T, et al. Multiple pathways coordinating reprogramming of endothelial cells into osteoblasts by BMP4. iScience 2021;24:102388 [PubMed: 33981975]

Author Manuscript Author Manuscript Author Manuscript Author Manuscript


29. Pan T, Martinez M, Hubka KM, Song JH, Lin SC, Yu G, et al. Cabozantinib Reverses Renal Cell Carcinoma-mediated Osteoblast Inhibition in Three-dimensional Coculture In Vitro and Reduces Bone Osteolysis In Vivo. Molecular cancer therapeutics 2020;19:1266–78 [PubMed: 32220969]
30. Walter-Yohrling J, Morgenbesser S, Rouleau C, Bagley R, Callahan M, Weber W, et al. Murine endothelial cell lines as models of tumor endothelial cells. Clin Cancer Res 2004;10:2179–89 [PubMed: 15041739]
31. Arbiser JL, Moses MA, Fernandez CA, Ghiso N, Cao Y, Klauber N, et al. Oncogenic H-ras stimulates tumor angiogenesis by two distinct pathways. Proc Natl Acad Sci U S A 1997;94:861–6 [PubMed: 9023347]
32. Foster BA, Gingrich JR, Kwon ED, Madias C, Greenberg NM. Characterization of prostatic epithelial cell lines derived from transgenic adenocarcinoma of the mouse prostate (TRAMP) model. Cancer Res 1997;57:3325–30 [PubMed: 9269988]
33. Watson PA, Ellwood-Yen K, King JC, Wongvipat J, Lebeau MM, Sawyers CL. Context-dependent hormone-refractory progression revealed through characterization of a novel murine prostate cancer cell line. Cancer research 2005;65:11565–71 [PubMed: 16357166]
34. Cao Y, Wang C, Zhang X, Xing G, Lu K, Gu Y, et al. Selective small molecule compounds increase BMP-2 responsiveness by inhibiting Smurf1-mediated Smad1/5 degradation. Scientific reports 2014;4:4965 [PubMed: 24828823]
35. Wu ZQ, Li XY, Hu CY, Ford M, Kleer CG, Weiss SJ. Canonical Wnt signaling regulates Slug activity and links epithelial-mesenchymal transition with epigenetic Breast Cancer 1, Early Onset (BRCA1) repression. Proceedings of the National Academy of Sciences of the United States of America 2012;109:16654–9 [PubMed: 23011797]
36. Teixeira CC, Liu Y, Thant LM, Pang J, Palmer G, Alikhani M. Foxo1, a novel regulator of osteoblast differentiation and skeletogenesis. The Journal of biological chemistry 2010;285:31055–65 [PubMed: 20650891]
37. Yang J, Li X, Li Y, Southwood M, Ye L, Long L, et al. Id proteins are critical downstream effectors of BMP signaling in human pulmonary arterial smooth muscle cells. Am J Physiol Lung Cell Mol Physiol 2013;305:L312–21 [PubMed: 23771884]
38. Hollnagel A, Oehlmann V, Heymer J, Ruther U, Nordheim A. Id genes are direct targets of bone morphogenetic protein induction in embryonic stem cells. J Biol Chem 1999;274:19838–45 [PubMed: 10391928]
39. Korchynskyi O, ten Dijke P. Identification and functional characterization of distinct critically important bone morphogenetic protein-specific response elements in the Id1 promoter. J Biol Chem 2002 277:4883–91. [PubMed: 11729207]
40. Min H, Danilenko DM, Scully SA, Bolon B, Ring BD, Tarpley JE, et al. Fgf-10 is required for both limb and lung development and exhibits striking functional similarity to Drosophila branchless. Genes Dev 1998;12:3156–61 [PubMed: 9784490]
41. Sekine K, Ohuchi H, Fujiwara M, Yamasaki M, Yoshizawa T, Sato T, et al. Fgf10 is essential for limb and lung formation. Nat Genet 1999;21:138–41 [PubMed: 9916808]
42. Midwood KS, Hussenet T, Langlois B, Orend G. Advances in tenascin-C biology. Cellular and molecular life sciences : CMLS 2011;68:3175–99 [PubMed: 21818551]
43. Corren J, Ziegler SF. TSLP: from allergy to cancer. Nat Immunol 2019;20:1603–9 [PubMed: 31745338]
44. Siddikuzzaman, Guruvayoorappan C, Berlin Grace VM. All trans retinoic acid and cancer. Immunopharmacol Immunotoxicol 2011;33:241–9 [PubMed: 20929432]
45. Lee YC, Lin SC, Yu G, Zhu M, Song JH, Rivera K, et al. Prostate tumor-induced stromal reprogramming generates Tenascin C that promotes prostate cancer metastasis through YAP/TAZ inhibition. Oncogene 2022;41:757–69 [PubMed: 34845375]
46. Pan T, Lin SC, Lee YC, Yu G, Song JH, Pan J, et al. Statins reduce castration-induced bone marrow adiposity and prostate cancer progression in bone. Oncogene 2021;40:4592–603 [PubMed: 34127814]
47. Pignolo R AM M, Baujat G, Berglund S, Cheung A, De Cunto C, Delai P, Di Rocco M, Haga N, Hsiao E, Kannu P, Keen R, Mancilla E, Grogan D, Marino R, Strahs A&Kaplan F.

Author Manuscript Author Manuscript Author Manuscript Author Manuscript

Palovarotene(PVO) for fibrodysplasia progressiva (FOP): data from the phase III MOVE trial. ASBMR Virtual Meeting 2020;11-15 September

48. Trump DL, Smith DC, Stiff D, Adedoyin A, Day R, Bahnson RR, et al. A phase II trial of all-trans-retinoic acid in hormone-refractory prostate cancer: a clinical trial with detailed pharmacokinetic analysis. Cancer Chemother Pharmacol 1997;39:349–56 [PubMed: 9025776]
49. Hind M, Stinchcombe S. Palovarotene, a novel retinoic acid receptor gamma agonist for the treatment of emphysema. Curr Opin Investig Drugs 2009;10:1243–50
50. Supakul S, Yao K, Ochi H, Shimada T, Hashimoto K, Sunamura S, et al. Pericytes as a Source of Osteogenic Cells in Bone Fracture Healing. Int J Mol Sci 2019;20
51. Yen YT, Chien M, Wu PY, Hung SC. PP2A in LepR+ mesenchymal stem cells contributes to embryonic and postnatal endochondral ossification through Runx2 dephosphorylation. Commun Biol 2021;4:658 [PubMed: 34079065]
52. Zhou BO, Yue R, Murphy MM, Peyer JG, Morrison SJ. Leptin-receptor-expressing mesenchymal stromal cells represent the main source of bone formed by adult bone marrow. Cell Stem Cell 2014;15:154–68 [PubMed: 24953181]
53. Shi Y, He G, Lee WC, McKenzie JA, Silva MJ, Long F. Gli1 identifies osteogenic progenitors for bone formation and fracture repair. Nat Commun 2017;8:2043 [PubMed: 29230039]
54. Tabatabai TS, Haji-Ghasem-Kashani M, Nasiri M. In vitro osteogenic induction of human adipose stem cells co-treated with betaine/osteogenesis differentiation medium. Mol Biol Res Commun 2021;10:93–103 [PubMed: 34316496]
55. Lin DPL, Dass CR. Transdifferentiation of adipocytes to osteoblasts: potential for orthopaedic treatment. J Pharm Pharmacol 2018;70:307–19 [PubMed: 29365349]
56. Cruz ACC, Cardozo F, Magini RS, Simoes CMO. Retinoic acid increases the effect of bone morphogenetic protein type 2 on osteogenic differentiation of human adipose-derived stem cells. J Appl Oral Sci 2019;27:e20180317 [PubMed: 30810639]
57. Gao M, Ossowski L, Ferrari AC. Activation of Rb and decline in androgen receptor protein precede retinoic acid-induced apoptosis in androgen-dependent LNCaP cells and their androgen-independent derivative. J Cell Physiol 1999;179:336–46 [PubMed: 10228952]
58. Lin E, Chen MC, Huang CY, Hsu SL, Huang WJ, Lin MS, et al. All-trans retinoic acid induces DU145 cell cycle arrest through Cdk5 activation. Cell Physiol Biochem 2014;33:1620–30 [PubMed: 24851929]
59. Chen MC, Huang CY, Hsu SL, Lin E, Ku CT, Lin H, et al. Retinoic Acid Induces Apoptosis of Prostate Cancer DU145 Cells through Cdk5 Overactivation. Evid Based Complement Alternat Med 2012;2012:580736 [PubMed: 23304206]
60. Kini AR, Peterson LA, Tallman MS, Lingen MW. Angiogenesis in acute promyelocytic leukemia: induction by vascular endothelial growth factor and inhibition by all-trans retinoic acid. Blood 2001;97:3919–24 [PubMed: 11389035]
61. Engblom C, Pfirschke C, Zilionis R, Da Silva Martins J, Bos SA, Courties G, et al. Osteoblasts remotely supply lung tumors with cancer-promoting SiglecF(high) neutrophils. Science 2017;358
62. Larange A, Cheroutre H. Retinoic Acid and Retinoic Acid Receptors as Pleiotropic Modulators of the Immune System. Annu Rev Immunol 2016;34:369–94 [PubMed: 27168242]

Author Manuscript Author Manuscript Author Manuscript Author Manuscript

## Statement of Significance

This study provides mechanistic insights into how retinoic acid receptor agonists suppress prostate cancer-induced bone formation and offers a rationale for developing retinoic acid receptor agonists for prostate cancer bone metastasis therapy.

Author Manuscript Author Manuscript Author Manuscript Author Manuscript

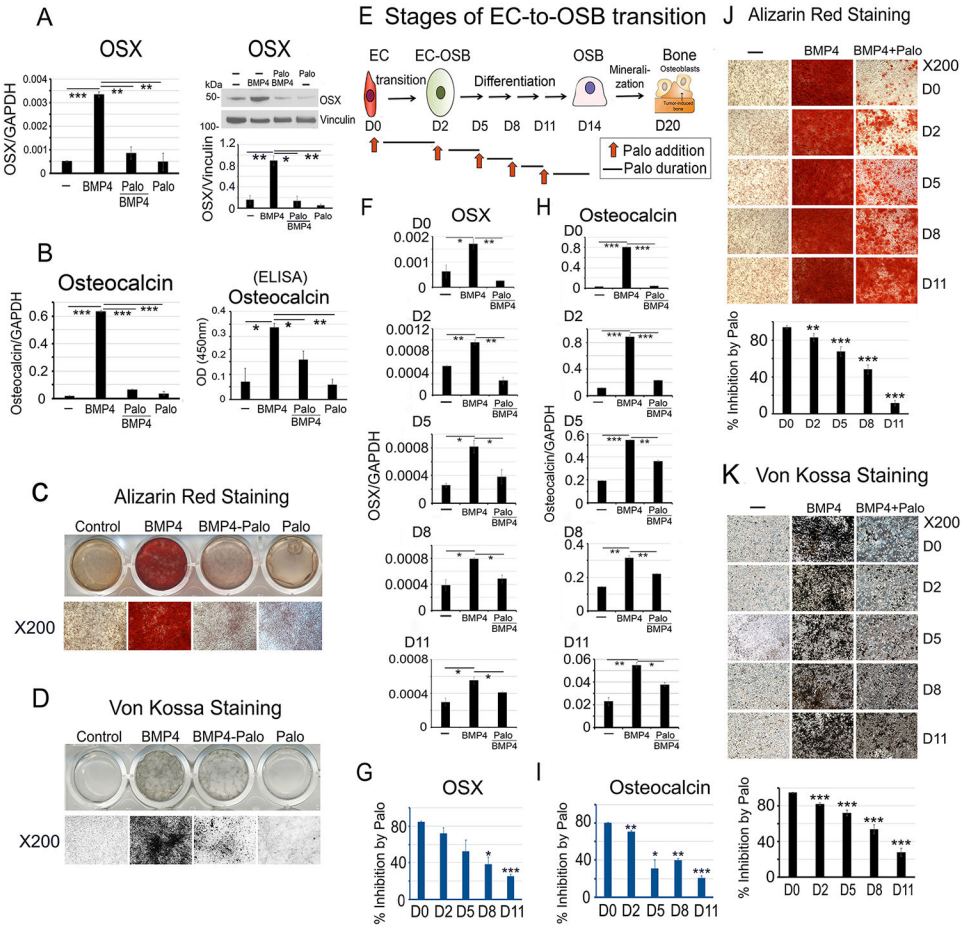


**Figure 1. Palovarotene inhibits BMP4-induced EC-to-OSB transition in 2H11 cells.**

(A-D) 2H11 ECs were treated with BMP4 (100 ng/mL) to induce EC-to-OSB transition. Palovarotene (Palo, 1 μM) effects were measured on (A) OSX mRNA (qRT-PCR) and protein (blot), (B) osteocalcin mRNA and protein (ELISA of conditioned medium), and mineralization by (C) Alizarin Red and (D) von Kossa staining. (E) Stages of EC-to-OSB transition. Red arrows, Palo addition at different times followed by a 3-day incubation. (F) OSX mRNA expression when Palo was added at D0, D2, D5, D8 or D11. (G) Percent inhibition of OSX expression by Palo in cells in (F) when compared to BMP4-treated only, using the formula 100-[(BMP4+Palo)/BMP4]x100. (H) Osteocalcin mRNA expression in cells treated as in (F). (I) Percent inhibition of osteocalcin expression by Palo as in (G). (J) Palo on mineralization when added at indicated days, as determined by Alizarin Red or (K) von Kossa staining. Staining quantified using ImageJ. *p<0.05, **p<0.01, ***p<0.001 by Students *t*-test in this and subsequent figures.

Author Manuscript Author Manuscript Author Manuscript Author Manuscript

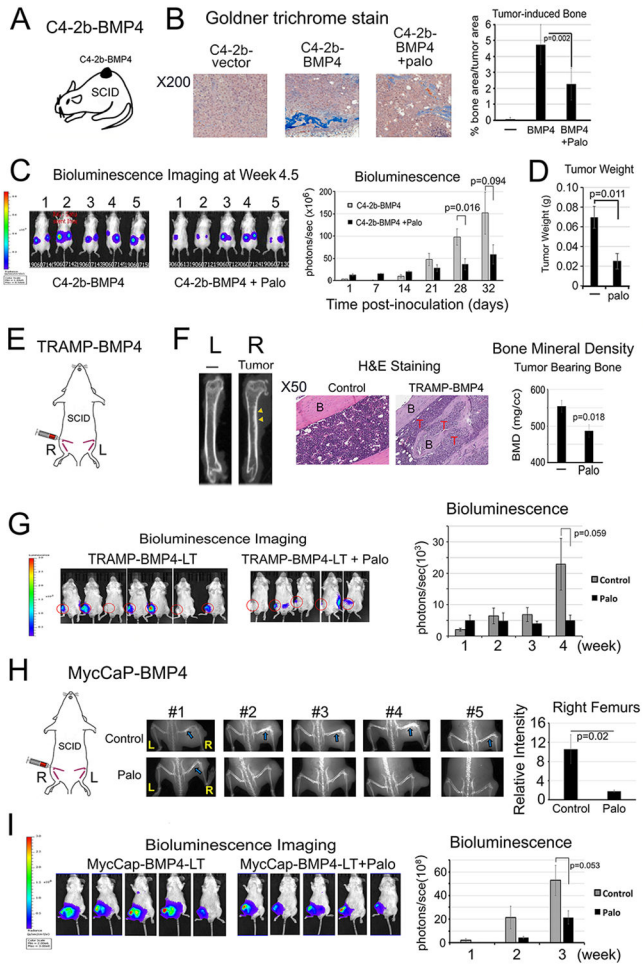


**Figure 2. Palovarotene reduces PCa-induced bone formation and tumor growth in SCID mice.**

(A) C4-2b-BMP4 subcutaneous implantation. (B) Goldner Trichrome staining of C4-2b-BMP4 tumors quantified using ImageJ. (C) Tumor size measurement by BLI in mice with C4-2b-BMP4 tumors. (D) Tumor weight at the termination of the study. Control (n=5), Palo-treated (n=5). (E) TRAMP-BMP4 intrabone injection. (F) MicroCT of femurs with or without TRAMP-BMP4 tumors (left). Histology of TRAMP-BMP4-induced bone compared with the non-tumor bearing bone (middle). B(bone), T(tumor). Palo on bone mineral density of tumor-bearing femurs (right). (G) TRAMP-BMP4 tumor size by BLI. Control (n=7); Palo-treated (n=5). (H) MycCaP-BMP4 intrabone injection (left). X-Ray of osteoblastic bone response induced by MycCaP-BMP4 in femurs with or without Palo (middle) and relative intensity quantified by ImageJ (right). Blue arrows, tumor bearing bone in the control group. (I) MycCaP-BMP4 tumor size by BLI. Control (n=5); Palo-treated (n=5).

Author Manuscript Author Manuscript Author Manuscript Author Manuscript

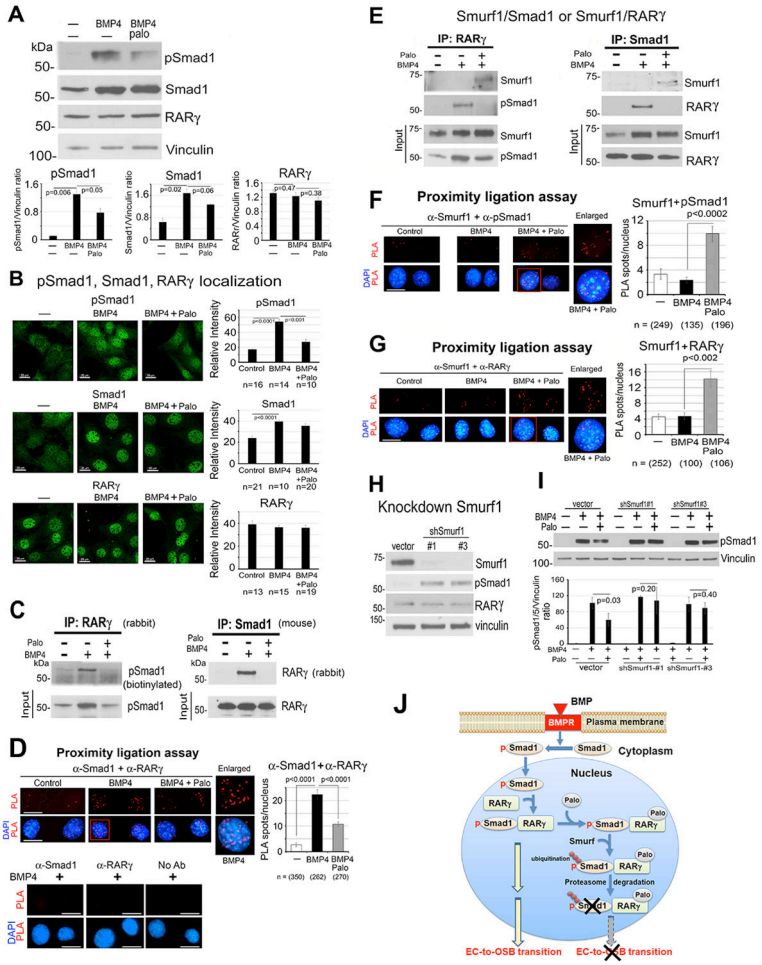


**Figure 3. Palovarotene decreases BMP4-stimulated pSmad1.**

(A) pSmad1, Smad1 and RARγ protein levels in 2H11 cells treated as indicated for 6 h. Vinculin, loading control. Blots quantified by ImageJ. (B) Immunofluorescence of pSmad1, Smad1, and RARγ in nucleus of cells in (A). Relative intensity quantified by ImageJ. n, number of nuclei examined. All bars, 20 μm. (C) Co-immunoprecipitation of RARγ and pSmad1 from nuclear extracts. (D) Proximity ligation assay for the interaction of RARγ and pSmad1. Red spots, PLA signals in the nucleus using anti-Smad1 and anti-RARγ antibodies. Single or no antibodies were used as controls. (E) Co-immunoprecipitations of Smurf1 with RARγ or pSmad1 using nuclear extracts. Note in (C, E), efficiency of immunoprecipitations could not be assessed due to RARγ and Smad1 being similar in size as IgG bands. (F-G) PLA for Smurf1 with pSmad1 (F) or RARγ (G). (H) Smurf1 knockdown in 2H11-shSmurf1#1 or #3 clones. (I) pSmad1 levels in 2H11-shSmurf1 clones. (J) Graphical summary. BMP4 stimulates an increase in pSmad1 that translocates into the nucleus, where pSmad1 and RARγ form a complex. Palo results in the recruitment of E3-ubiquitin ligase Smurf1 to the pSmad1/RARγ complex, leading to pSmad1 degradation and inhibition of EC-to-OSB transition.

Author Manuscript Author Manuscript Author Manuscript Author Manuscript

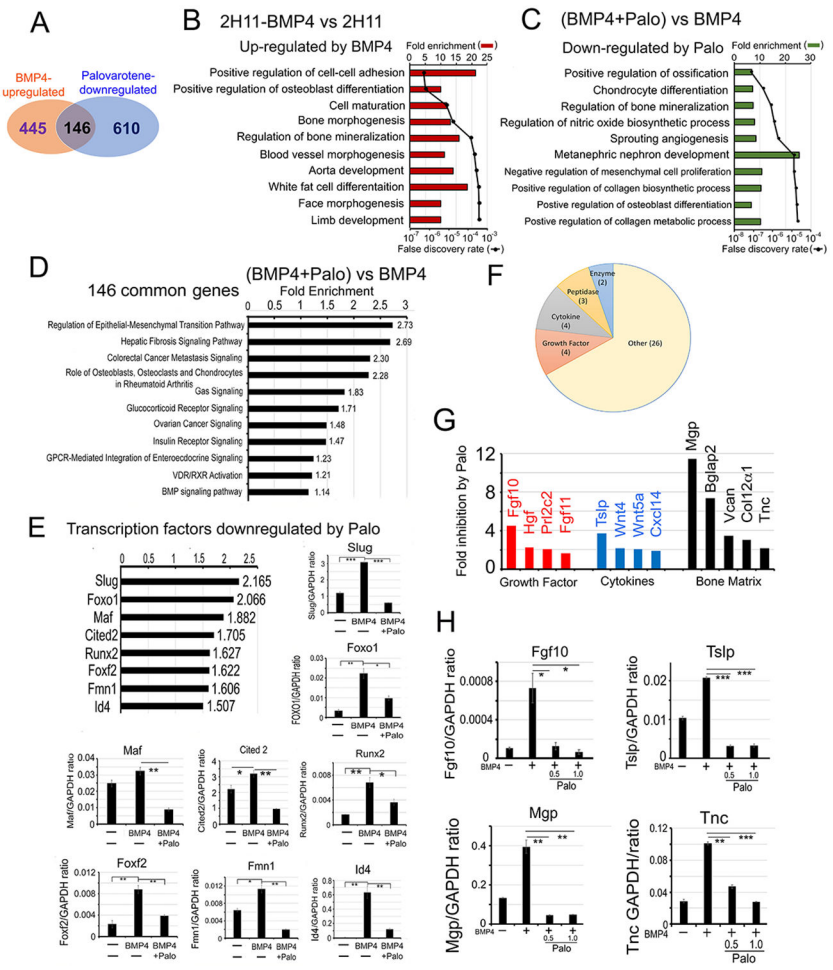


**Figure 4. Palovarotene alters the BMP4-induced transcriptome.**

(A) Venn diagram of number of genes whose expression levels are upregulated by BMP4 and downregulated by Palo in 2H11 cells. Pathway analyses of genes upregulated by BMP4 (B), downregulated by Palo after 48 h (C), and up-regulated by BMP4 but down-regulated by Palo (Palo-regulated genes) (D). (E) Transcription factors upregulated by BMP4 and downregulated by Palo. qRT-PCR for indicated mRNAs. (F) Category of BMP4-inducible secreted proteins that are inhibited by Palo. (G) BMP4-stimulated secreted proteins (termed “osteocrines”) (12) that are decreased by Palo. (H) qRT-PCR for select mRNAs in (G) treated as indicated.

Author Manuscript Author Manuscript Author Manuscript Author Manuscript

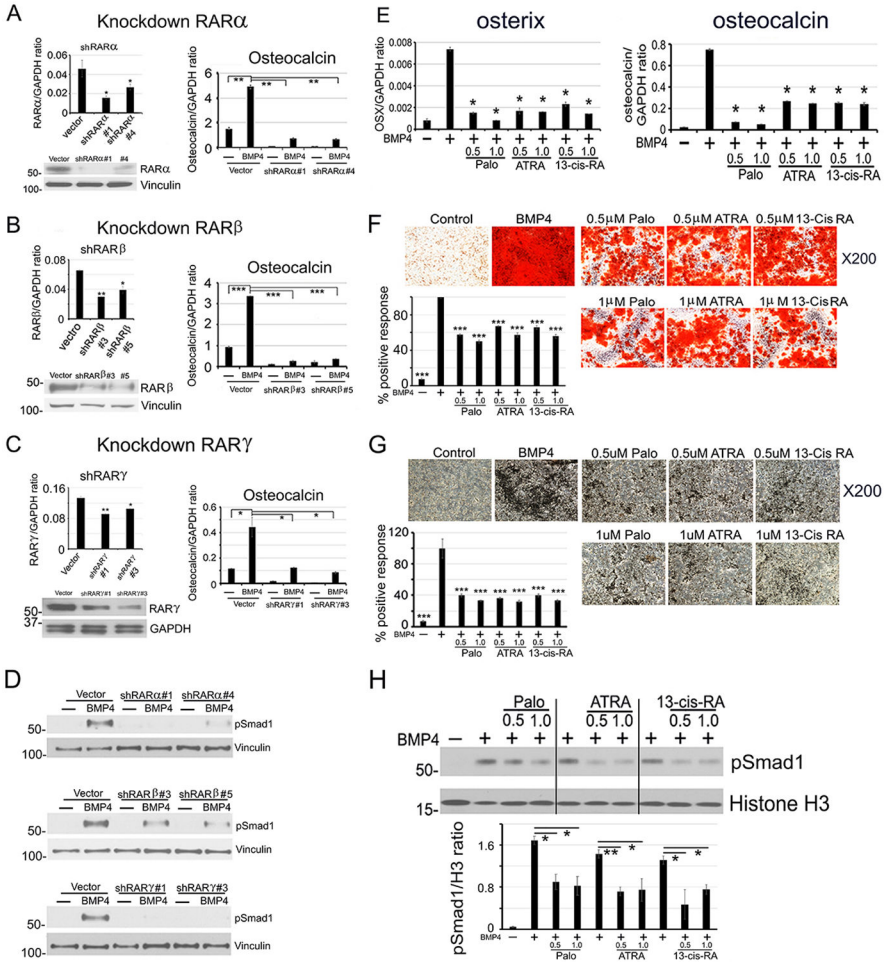


**Figure 5. All three RAR isoforms are involved in EC-to-OSB transition.**

(A-C) (Left) RARα, RARβ, or RARγ knockdown in 2H11 cells by shRNA (qRT-PCR and western blot). (Right) RAR knockdowns on BMP4-stimulated osteocalcin expression (qRT-PCR). (D) RAR knockdowns on BMP4-stimulated nuclear pSmad1 at 48 h. (E-G) ATRA or 13-cis-RA on BMP4-stimulated osterix and osteocalcin expression (E), mineralization measured by Alizarin Red (F), or von Kossa (G) staining. (H) pSmad1 levels BMP4-stimulated 2H11 cells treated with Palo, ATRA or 13-cis-RA at 48 h. Histone H3, nuclear protein loading control. All samples were run on the same gel.

Author Manuscript Author Manuscript Author Manuscript Author Manuscript

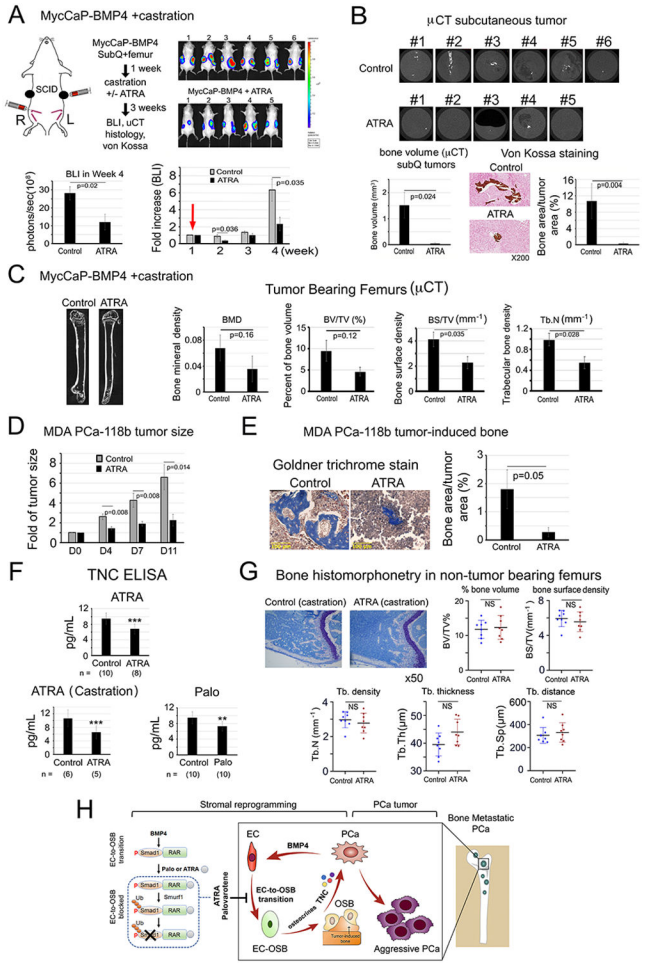


**Figure 6. ATRA reduces PCa-induced bone formation and tumor growth of MycCaP-BMP4 and MDA PCa-118b tumors, reduces plasma TNC levels, but does not lead to overall bone loss in non-tumor bearing femur in castrated mice.**

(A) MycCaP-BMP4 cells (0.25 x$10^6$/site) were implanted subcutaneously and intrafemorally. Mice were castrated 1-week post-implantation (red arrow) and treated 3-weeks with or without ATRA. Tumor size measured by BLI. Control (n=6); ATRA-treated (n=5). (B) μCT of ectopic bone in tumors grown subcutaneously. Mineralization by von Kossa staining. (C) μCT of tumor-bearing femurs from mice in (A). (D) Tumor size of MDA PCa-118b with or without ATRA. Control (n=7); ATRA-treated (n=7). (E) Mineralization by Goldner Trichrome staining. (F) Serum TNC protein levels from SCID mice treated with ATRA, ATRA+castration, or Palo were quantified by ELISA. n, number of mice analyzed. (G) Bone histomorphometry on non-tumor containing femurs from ATRA plus castration-treated mice in (A). (H) Model. Within the tumor microenvironment, PCa-induced bone originates from ECs that have undergone EC-to-OSB transition in response to PCa-secreted BMP4 signaling through a pSmad1/RAR pathway (boxed). Activation of RARs by Palo or ATRA inhibits BMP4-mediated EC-to-OSB transition through a non-canonical RAR/pSmad1/Smurf1 pathway that results in pSmad1 degradation (dotted). This Palo/ATRA-mediated inhibitory pathway blocks stromal reprogramming and leads to a decrease in

Author Manuscript Author Manuscript Author Manuscript Author Manuscript

EC-OSB cell secreted factors (“osteocrines”) including TNC, a reduction in PCa-induced aberrant bone formation, and a decrease in metastatic PCa tumor growth in bone.